Supporting Information

Water-Resistant Organic-Inorganic Hybrid Perovskite Quantum Dots Activated by Electron-Deficient d-Orbital of Platinum Atoms for Nitrogen Fixation

Yixuan Gao[a]#, Xiao Su[a]#, Juanjuan Wei[a]#, Jianghui Sun, Min Zhang, Hongwei Tan*[a], Jiangwei Zhang*[b], Jin Ouyang[a], Na Na*[a]

Key Laboratory of Radiopharmaceuticals, Ministry of Education, College of Chemistry, Beijing Normal University, Beijing 100875, China.

# These authors contributed equally to this work.

*Corresponding Author: nana@bnu.edu.cn

Reagent

The chemical reagents used in the experiment are list as follows: Polycarbonate resin (PC, M.W. 45000, Acros), Methylamine hydrobromide (CH_3NH_3Br, MABr, 98%, Innochem), Lead (II) bromide ($PbBr_2$, Puratronic, 99.9%, Macklin), N, N-dimethylformamide (DMF, 99.9%, extra dry, Innochem), H_2PtCl_6 (99.9%, Macklin), K_2PtCl_4 (99.9%, Macklin), $C_4H_8O_4Zn$ (Macklin, AR). Ultrapure water (Mill-Q, Millipore, 18.2 MΩ) was used in all experiments. All chemicals were used without further purification.

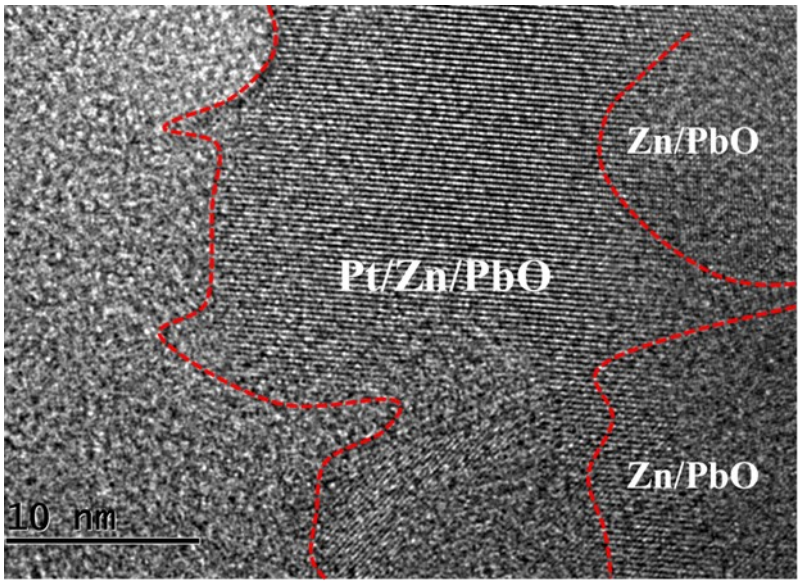

Fig. S1. HRTEM characterization of Pt^{IV}/Zn/PbO/PC-Zn/$MAPbBr_3$.

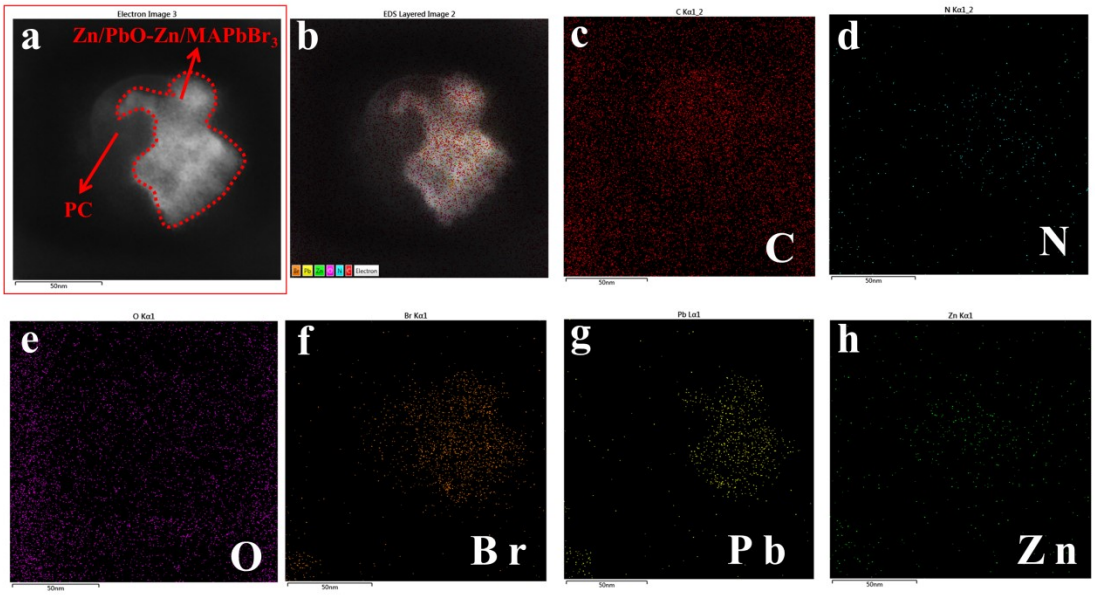

Fig. S2. HAADF-STEM of the Zn/PbO/PC-Zn/$MAPbBr_3$ with elemental mapping images of C, N, O, Br, Pb and Zn (a-h). Zn/PbO-Zn/$MAPbBr_3$ and PC were labeled in (a).

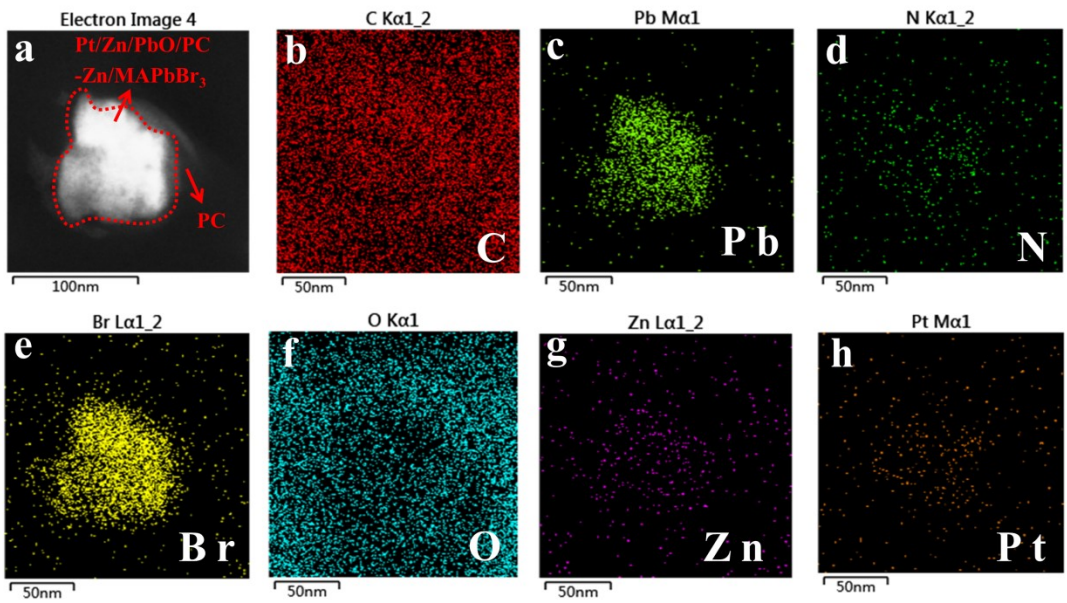

Fig. S3. HAADF-STEM of the Pt^{IV}/Zn/PbO/PC-Zn/$MAPbBr_3$ with elemental mapping images of C, Pb, N, Br, O, Zn and Pt (a-h). Pt^{IV}/Zn/PbO-Zn/$MAPbBr_3$ and PC were labeled in (a).

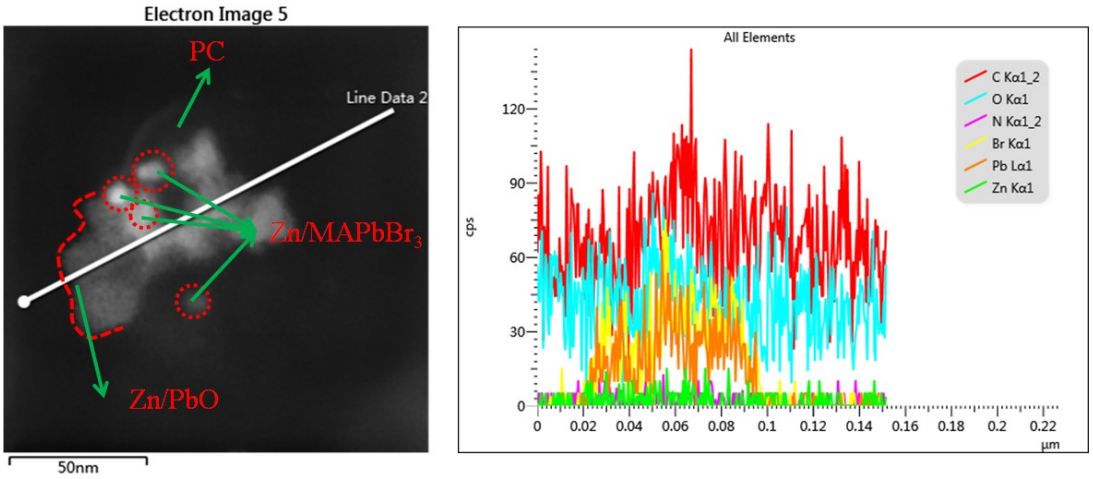

Fig. S4. HAADF-STEM (a) of the Zn/PbO/PC-Zn/$MAPbBr_3$ with EDX (b) line-scanning profile curves.

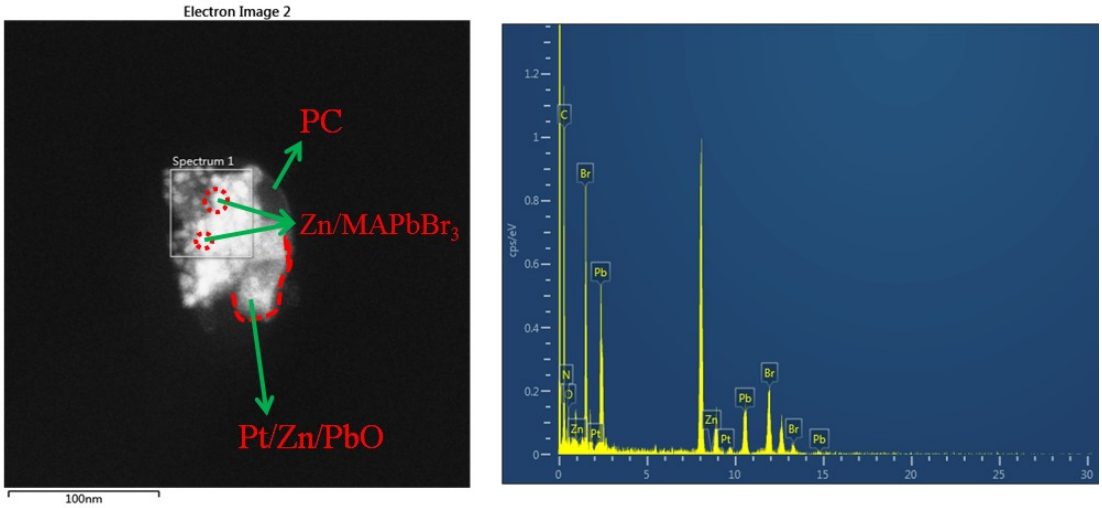

Fig. S5. HAADF-STEM (a) of the Pt^{IV}/Zn/PbO/PC-Zn/$MAPbBr_3$ with the EDX (b)spectrum.

Table S1. The assignments of FTIR peaks for PbO/PC-$MAPbBr_3$, Zn/PbO/PC-Zn/$MAPbBr_3$ and Pt^{IV}/Zn/PbO/PC-Zn/$MAPbBr_3$.

1775 cm^{-1}	stretching vibration of C=O
1504、1463 cm^{-1}	flexural vibration of -C=C- of benzene rings
1365 cm^{-1}	flexural vibration of -C(CH_3)
1228、1192、1163 cm^{-1}	stretching vibration of -C-O-C-
1601、1492 cm^{-1}	bending vibration of -C=C- of benzene rings
1079、1016 cm^{-1}	In-plane deformation of =C of Para-substituted benzene rings
830 cm^{-1}	out-of-plane deformation of =C of Para-substituted benzene rings

Table S2. The assignments of Raman peaks for PbO/PC-$MAPbBr_3$, Zn/PbO/PC-Zn/$MAPbBr_3$ and Pt^{IV}/Zn/PbO/PC-Zn/$MAPbBr_3$.

637、1231 cm^{-1}	stretching vibrations of central carbon atom between the two benzene rings and the carbon atoms of the benzene ring (-C-C=)
707 cm^{-1}	bending vibration between atoms of carbon chain in benzene ring (-C=C-)
887 cm^{-1}	asymmetric stretching vibration (-C-O-C-)
1105 cm^{-1}	stretching vibrations of -C=C-C= of benzene rings
1175 cm^{-1}	stretching vibration of C=O
1590 cm^{-1}	asymmetric stretching vibration of =C of benzene rings

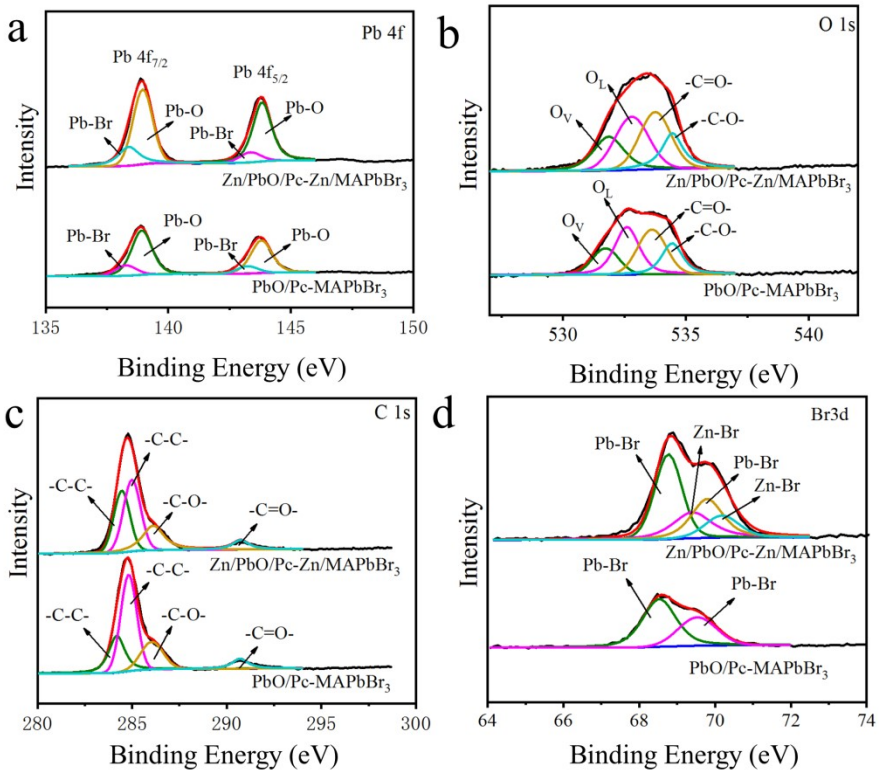

Fig. S6. XPS spectra of the Pb4f (a), O1s (b), C1s (c) and Br3d (d) of the PbO/PC-$MAPbBr_3$ and Zn/PbO/PC-Zn/$MAPbBr_3$.

In Pb4f XPS spectra (Fig S6a), Pb-O and Pb-Br peaks were detected in both PbO/PC-$MAPbBr_3$ and Zn/PbO/PC-Zn/$MAPbBr_3$. Notably, on surface of Zn/PbO/PC-Zn/$MAPbBr_3$ and PbO/PC-$MAPbBr_3$, Pb-O signal was much higher than that of Pb-Br (from the subsurface of $MAPbBr_3$ and Zn/$MAPbBr_3$). This indicated that more PbO was exposed on the material surface. These Zn/PbO exposed surface would subsequently provide more active sites to interact with N_2 for photocatalysis NRR. In addition, C-1s peaks of PC (Fig S6c, Table S3) also confirmed the encapsulation by PC. Therefore, the present Zn/PbO/PC-Zn/$MAPbBr_3$ nanomaterials were further confirmed to be covered by PC with more Zn/PbO exposed on the surface. Besides, quite weak Br(3d) peaks of Br(3d5/2) and Br(3d7/2) for both Zn/PbO/PC-Zn/$MAPbBr_3$ and PbO/PC-$MAPbBr_3$ were observed in the subsurface (Fig 6d).

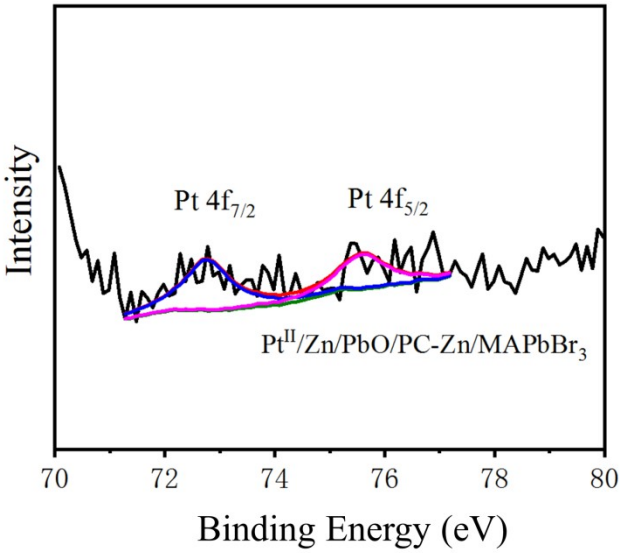

Fig. S7. X-ray photoelectron spectroscopy (XPS) spectra of the Pt^{II} 4f (d) of the Pt^{II}/Zn/PbO/PC-Zn/$MAPbBr_3$

Table S3. Polycarbonate structure and bond assignments of PbO/PC-$MAPbBr_3$, Zn/PbO/PC-Zn/$MAPbBr_3$ and Pt^{IV}/Zn/PbO/PC-Zn/$MAPbBr_3$ in XPS peaks.

Peak	Polycarbonate Structure
-C-C-	Aromatic C-C/C-H
-C-C-	Aliphatic C-C/C-H
-C-O-	Aromatic C-O
-C=O-	Carbonate O-(C=O)-O
-C-N	$MAPbBr_3$ PQDs -C-N

Table S4. PL Decay Parameters of the PbO/PC-$MAPbBr_3$, Zn/PbO/PC-Zn/$MAPbBr_3$ and Pt^{IV}/Zn/PbO/PC-Zn/$MAPbBr_3$ composite.

	τ_1(ns)	τ_2(ns)	$\tau_{average}$(ns)	χ
PbO/PC-$MAPbBr_3$	9	50	27.76	1.24
Zn/PbO/PC-Zn/$MAPbBr_3$	8	36	18.01	1.28
Pt^{IV}/Zn/PbO/PC-Zn/$MAPbBr_3$	6.7	25.1	13.70	1.18

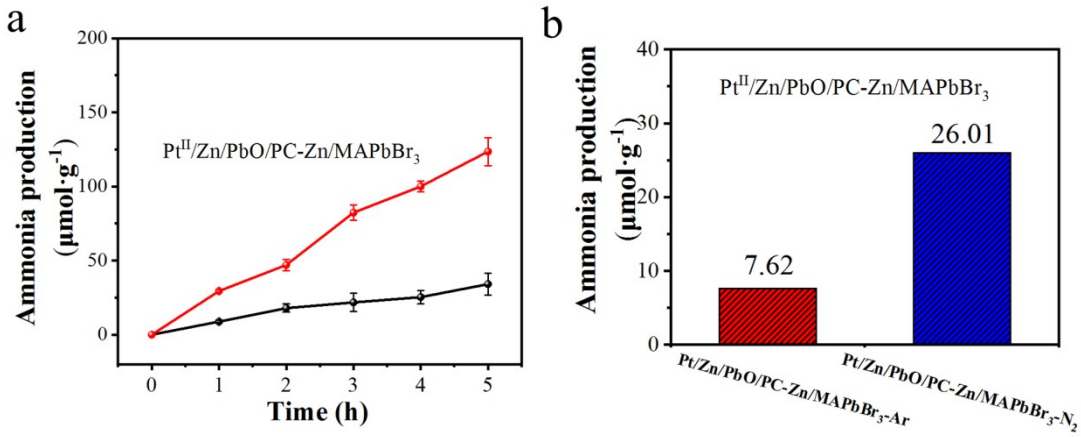

Fig. S8. Evaluation of photocatalytic NRR catalyzed by Pt^{II}/Zn/PbO/PC-Zn/$MAPbBr_3$. (a) NH_3 yield versus irradiation time with N_2 and Ar as feed gases. (b) Average NH_3 yields.

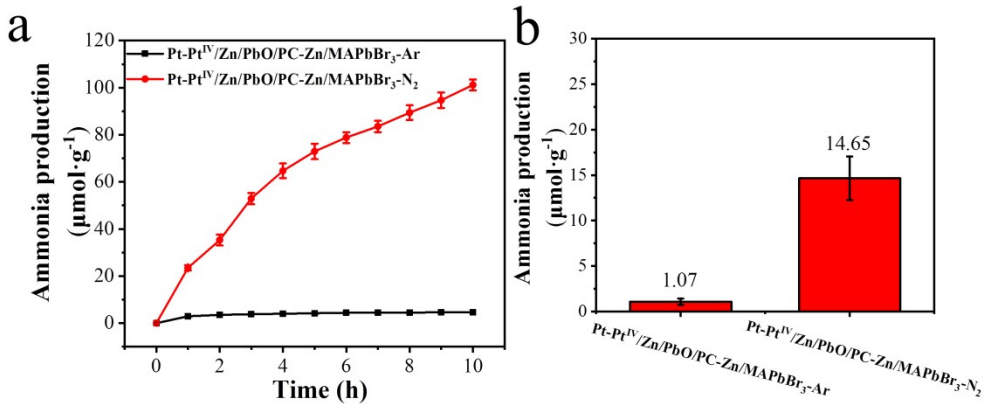

Fig. S9. Evaluation of photocatalytic NRR catalyzed by Pt nanoparticles catalyst loading (Pt-Pt^{IV}/Zn/PbO/PC-Zn/MAPbBr) on NRR performance. (a) NH_3 yield versus irradiation time with N_2 and Ar as feed gases. (b) Average NH_3 yields.

It should be noted, the present Pt^{IV}/Zn/PbO/PC-Zn/MAPbBr$_3$ exhibited the much higher NRR efficiency than the Pt-loaded nanoparticles (Pt-Pt^{IV}/Zn/PbO/PC-Zn/MAPbBr$_3$) (Figure S9), which could be caused by the stronger interaction between the loaded catalysts and H proton.

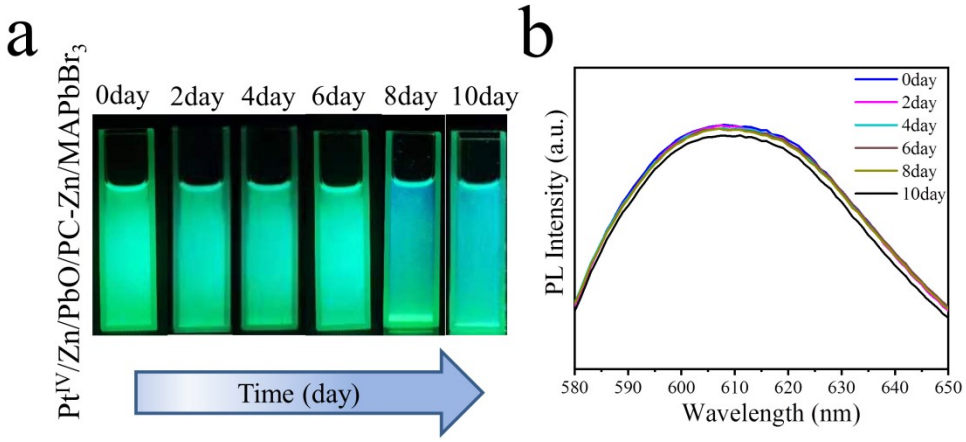

Fig. S10. FL characterizations on water-resistance and stability after photocatalytic NRR in aqueous phase for different days (0-10 days).

Table S5. Fitting results of impedance data of the PbO/PC-$MAPbBr_3$, Zn/PbO/PC-Zn/$MAPbBr_3$ and Pt^{IV}/Zn/PbO/PC-Zn/$MAPbBr_3$ before the stability test.

	$R_s(\Omega)$	$R_{sc}(\Omega)$	$R_{ct}(\Omega)$
PbO/PC-$MAPbBr_3$	41	491	34050
Zn/PbO/PC-Zn/$MAPbBr_3$	32	357	12271
Pt^{IV}/Zn/PbO/PC-Zn/$MAPbBr_3$	24	322	6071

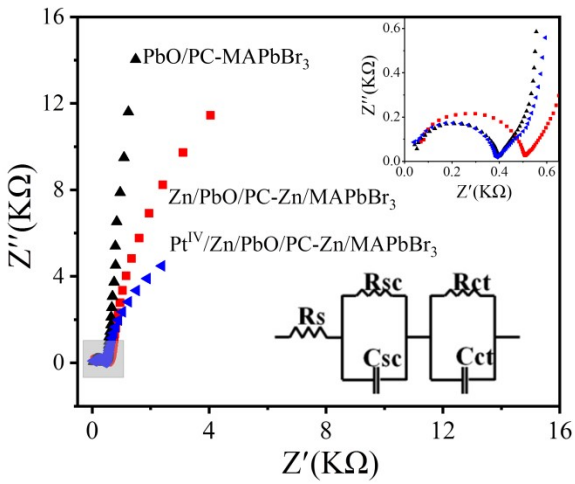

Fig. S11. The EIS spectra of the catalyst after the stability test.

Table S6. Fitting results of impedance data of the PbO/PC-$MAPbBr_3$, Zn/PbO/PC-Zn/$MAPbBr_3$ and Pt^{IV}/Zn/PbO/PC-Zn/$MAPbBr_3$ after the stability test.

	$R_s(\Omega)$	$R_{sc}(\Omega)$	$R_{ct}(\Omega)$
PbO/PC-$MAPbBr_3$	32	358	34050
Zn/PbO/PC-Zn/$MAPbBr_3$	42	422	13271
Pt^{IV}/Zn/PbO/PC-Zn/$MAPbBr_3$	24	358	6100

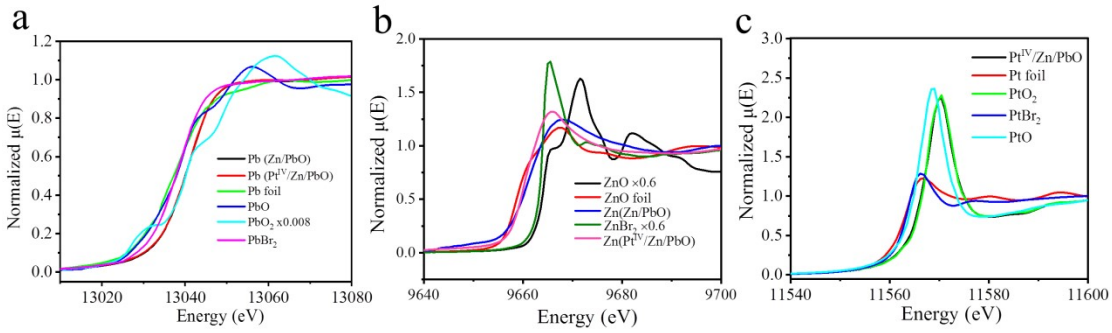

Fig. S12. Normalized K edge X-ray absorption near edge structure (XANES) χ(E) spectra of Zn (a), Pb (b) and Pt^{IV} (c).

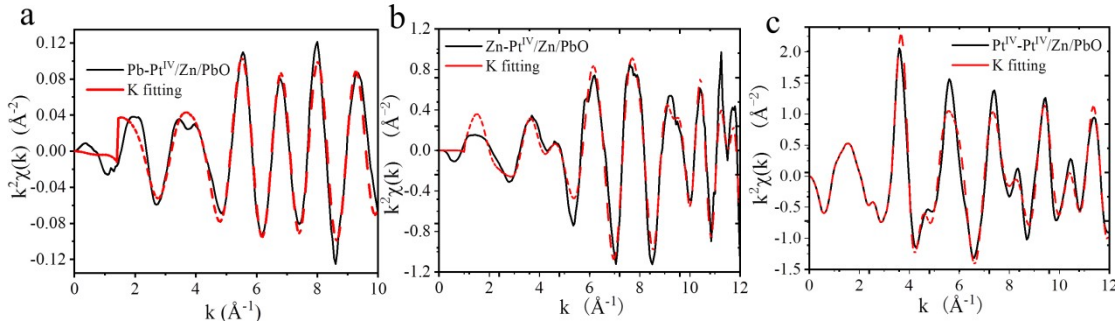

Fig. S13. k^2 χ(k) oscillations spectra of the PbO/PC-$MAPbBr_3$, Zn/PbO/PC-Zn/$MAPbBr_3$ and Pt^{IV}/Zn/PbO/PC-Zn/$MAPbBr_3$.

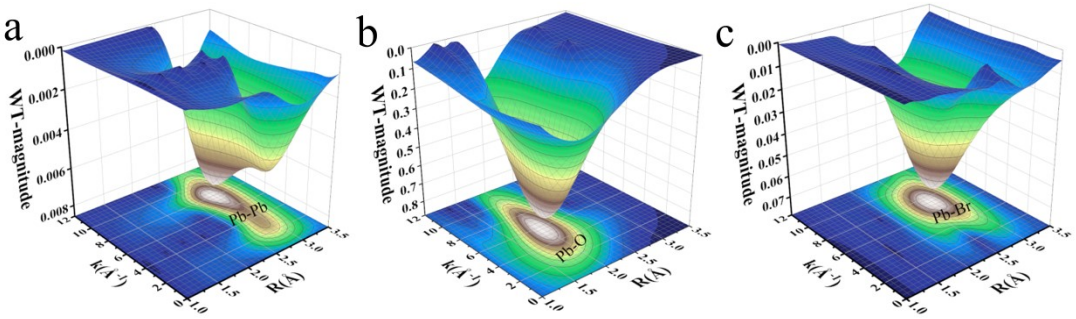

Fig. S14. Wavelet transformextended X-ray absorption fine structure (WTEXAFS) of Pb foil (d), PbO (e) and $PbBr_2$ (f).

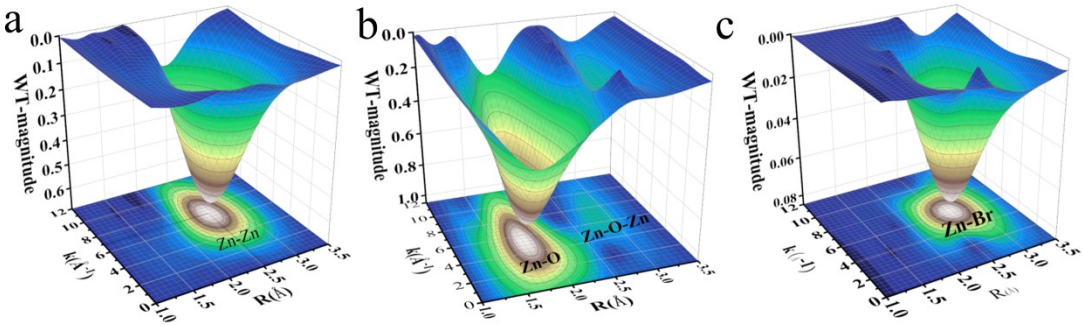

Fig. S15. Wavelet transformextended X-ray absorption fine structure (WTEXAFS) of Zn foil (a), ZnO (b) and $ZnBr_2$ (c).

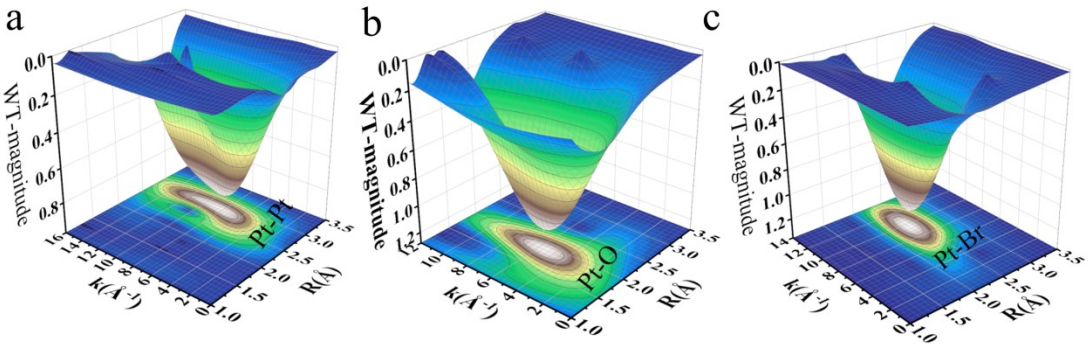

Fig. S16. Wavelet transformextended X-ray absorption fine structure (WTEXAFS) of Pt foil (a), PtO_2 (b) and $PtBr_2$ (c).

Table S7. Structural parameters extracted from the Zn K-edge χ(R) space spectra fitting of Pt^{IV}/Zn/PbO/PC-Zn/$MAPbBr_3$.

	Reduced Chi-square (χ_v^2)	R-factor（%）	amp/ S_0^2	$N_{(Zn-O\ path)}$	$R_{(Zn-O\ path)}$ (Å)	$\sigma^2_{(Zn-O\ path)}$ ($10^{-3}Å^2$)	ΔE_0 (eV)
Zn-Pt^{IV}/Zn/PbO	372.35	0.0’2877	0.884	2.46±0.23	1.809 ± 0.055	3.7+/-1.1	2.42+/- 1.24
				$N_{(Zn-Br\ path)}$	$R_{(Zn-Br\ path)}$ (Å)	$\sigma^2_{(Zn-Br\ path)}$ ($10^{-3}Å^2$)	ΔE_0 (eV)
				2.26±0.27	2.431 ± 0.068	4.5+/-1.3	3.06+/-1.22
				$N_{(Zn-O-Pb(Pt)\ path)}$	$R_{(Zn-O-Pb(Pt)\ path)}$	$\sigma^2_{(Zn-O-Pb(Pt)\ path)}$	ΔE_0 (eV)
				1.21±0.18	3.112± 0.087	6.6+/-3.6	5.03+/-3.37

Table S8. Structural parameters extracted from the Pb K-edge χ(R) space spectra fitting of Pt^{IV}/Zn/PbO/PCPC-Zn/$MAPbBr_3$.

	Reduced Chi-square (χ_v^2)	R-factor（%）	amp/ S_0^2	$N_{(Pb\text{-}O\ path)}$	$R_{(Pb\text{-}O\ path)}$ (Å)	$\sigma^2_{(Pb\text{-}O\ path)}$ (10^{-3}Å^2)	ΔE_0 (eV)
Pb-Pt^{IV}/Zn/PbO	2480.69	0.0407	0.852	2.24±0.17	2.163 ± 0.026	3.4+/-1.2	3.02+/-1.75
				$N_{(Pb\text{-}Br\ path)}$	$R_{(Pb\text{-}Br\ path)}$ (Å)	$\sigma^2_{(Pb\text{-}Br\ path)}$ (10^{-3}Å^2)	ΔE_0 (eV)
				3.64±0.43	2.904 ± 0.035	5.8+/-3.1	4.15+/-3.07

Table S9. Structural parameters extracted from the Pt K-edge χ(R) space spectra fitting of PtIV/Zn/PbO/PC-Zn/MAPbBr3.

	Reduced Chi-square (χ_v^2)	R-factor（%）	amp/ S_0^2	$N_{(Pt\text{-}O\ path)}$	$R_{(Pt\text{-}O\ path)}$ (Å)	$\sigma^2_{(Pt\text{-}O\ path)}$ ($10^{-3}Å^2$)	ΔE_0 (eV)
Pt-Pt^{IV}/Zn/PbO	508.43	0.0406	0.80+/-0.11	6	1.993± 0.056	3.1+/-1.7	3.43+/-1.01
			amp/ S_0^2	$N_{(Pt\text{-}O\text{-}Pt(Pb))}$	$R_{(Pt\text{-}O\text{-}Pt(Pb))}$ (Å)	$\sigma^2_{(Pt\text{-}O\text{-}Pt(Pb))}$ ($10^{-3}Å^2$)	ΔE_0 (eV)
			0.81+/-0.15	2	3.111 ± 0.088	5.5+/-2.6	4.71+/-2.21
			amp/ S_0^2	$N_{(Pt\text{-}O\text{-}Pt(Pb))}$	$R_{(Pt\text{-}O\text{-}Pt(Pb))}$ (Å)	$\sigma^2_{(Pt\text{-}O\text{-}Pt(Pb))}$ ($10^{-3}Å^2$)	ΔE_0 (eV)
			0.83+/-0.15	4	3.659± 0.125	5.5+/-2.6	4.71+/-2.21

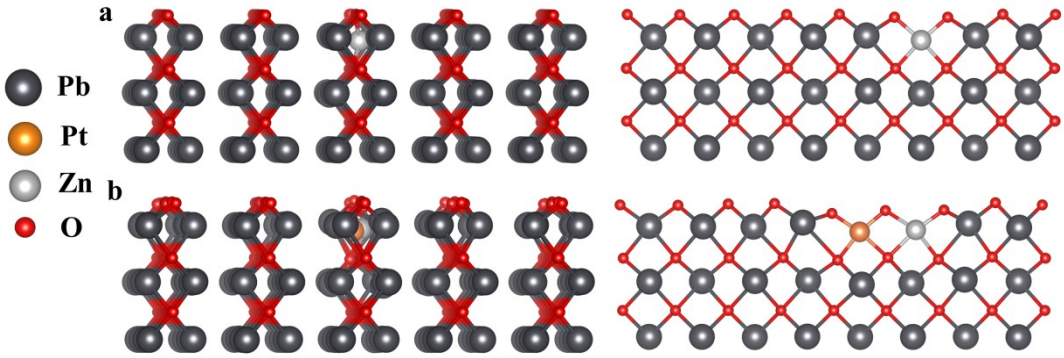

Fig. S17. The optimized structure of (a) Zn doped and (b) Zn/Pt^{IV} co-doped PbO (110) surface.

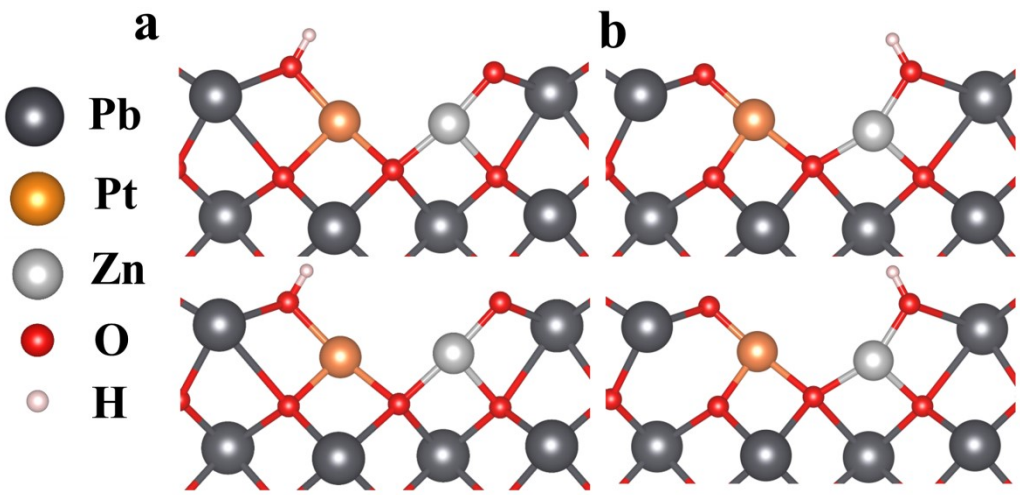

Fig. S18. The optimized structure of H adsorbed on (a) Pt^{IV} and (b) Zn site in neutral (above) or charged (below) system.